Agricultural and Forest Meteorology 260–261 (2018) 131–143

Contents lists available at ScienceDirect

Agricultural and Forest Meteorology

journal homepage: www.elsevier.com/locate/agrformet

Partitioning of evapotranspiration in remote sensing-based models

Carl J. Talsma[a,*], Stephen P. Good[a], Carlos Jimenez[b], Brecht Martens[c], Joshua B. Fisher[d], Diego G. Miralles[c], Matthew F. McCabe[e], Adam J. Purdy[f]

[a] Department of Biological & Ecological Engineering, Oregon State University, Corvallis, Oregon, USA
[b] Estellus, Paris, France
[c] Laboratory of Hydrology and Water Management, Ghent University, Ghent, Belgium
[d] Jet Propulsion Laboratory, California Institute of Technology, Pasadena, California, USA
[e] Division of Biological and Environmental Sciences and Engineering, King Abdullah University of Science and Technology, Thuwal, Saudi Arabia
[f] Department of Earth System Science, University of California, Irvine, California, USA

ARTICLE INFO

Keywords:
Evapotranspiration
Partitioning
Modeling
Remote sensing
Transpiration
Soil evaporation

ABSTRACT

Satellite based retrievals of evapotranspiration (ET) are widely used for assessments of global and regional scale surface fluxes. However, the partitioning of the estimated ET between soil evaporation, transpiration, and canopy interception regularly shows strong divergence between models, and to date, remains largely unvalidated. To examine this problem, this paper considers three algorithms: the Penman-Monteith model from the Moderate Resolution Imaging Spectroradiometer (PM-MODIS), the Priestley-Taylor Jet Propulsion Laboratory model (PT-JPL), and the Global Land Evaporation Amsterdam Model (GLEAM). Surface flux estimates from these three models, obtained via the WACMOS-ET initiative, are compared against a comprehensive collection of field studies, spanning a wide range of climates and land cover types. Overall, we find errors between estimates of field and remote sensing-based soil evaporation (RMSD = 90–114%, r^2 = 0.14–0.25, N = 35), interception (RMSD = 62–181%, r^2 = 0.39–0.85, N = 13), and transpiration (RMSD = 54–114%, r^2 = 0.33–0.55, N = 35) are relatively large compared to the combined estimates of total ET (RMSD = 35–49%, r^2 = 0.61–0.75, N = 35). Errors in modeled ET components are compared between land cover types, field methods, and precipitation regimes. Modeled estimates of soil evaporation were found to have significant deviations from observed values across all three models, while the characterization of vegetation effects also influences errors in all three components. Improvements in these estimates, and other satellite based partitioning estimates are likely to lead to better understanding of the movement of water through the soil-plant-water continuum.

1. Introduction

The evaporation of water from the Earth's surface to the atmosphere represents a critical link between the global water, carbon, and energy cycles (Oki and Kanae, 2006). An estimated two thirds of terrestrial rainfall returns to the atmosphere as evapotranspiration (ET) from the continents (Hobbins et al., 2004; Teuling et al., 2009) and the associated latent heat flux corresponds to a cooling of the Northern Hemisphere of about 15°–25 °C (Shukla and Mintz, 1982). ET is a critical process governing water resource availability, agricultural productivity, and irrigation efficiency, as well as impacting the severity of droughts, floods, and wildfires (Littell et al., 2016; Molden et al., 2010; Trenberth, 2011; Wallace, 2000). Furthermore, the energy flux associated with ET fundamentally influences the development of the planetary boundary layer and the atmospheric processes contained within it (Ek and Holtslag, 2004; Pielke et al., 1998; Seneviratne et al., 2010). Future climate warming is expected to significantly alter the global water cycle, affecting regional and global rates of ET, precipitation, and streamflow (Huntington, 2006; Zhang et al., 2016). Given the important role of ET in a variety of land surface processes, accurately estimating large-scale fluxes of ET is critical to our understanding of the earth system.

Spatially distributed, remote sensing-based ET models have become a dominant means to estimate catchment and global-scale ET fluxes (Anderson et al., 2007; Fisher et al., 2017; Schmugge et al., 2002). The large spatial extent and fine temporal resolution of these remote sensing products makes them perhaps the only observational means to assess global-scale impacts of changes in ET fluxes. These factors have made remote sensing-based models a powerful tool in both climate and large-scale hydrologic applications. Many of these remote sensing-based models estimate total ET via combination of its separate components: transpiration through plant stomata, soil evaporation from the top layer

* Corresponding author at: Gilmore Hall, 124 SW 26th St., Corvallis, OR 97331, USA.
E-mail address: talsmac83@gmail.com (C.J. Talsma).

https://doi.org/10.1016/j.agrformet.2018.05.010
Received 1 December 2017; Received in revised form 8 May 2018; Accepted 11 May 2018

of soil, and canopy rainfall interception. However, the wide array of algorithms and choice of forcing datasets have hampered the analysis of model results, as errors in model estimates may come from both forcing errors and/or errors in algorithms and parametrizations (Ershadi et al., 2015). Recent efforts have compared ET fluxes from several satellite-based ET models using a common forcing dataset, simplifying the comparison substantially (McCabe et al., 2016; Michel et al., 2016; Miralles et al., 2016).

These remote sensing-based ET estimates have shown good relative agreement in global estimates, but larger discrepancies regionally (Michel et al., 2016). Interestingly, the limited number of studies comparing individual ET components have shown that the global and regional contribution of transpiration, soil evaporation, and interception vary significantly between models, even where total ET estimates agree (Miralles et al., 2016). The divergence of ET partitioning estimates suggests that some models may contain large ET partitioning errors. Accurate partitioning estimates are highly desired for research related to agriculture, climate and land-use change, hydrology, and water resource availability. ET partitioning is also a crucial factor for global climate models as the partitioning of ET has proven to be a significant source of uncertainty for future climate projections (Lawrence et al., 2007). Incorrect parameterizations within ET models are likely to compromise the accuracy of estimates across ecoregions and through time. Furthermore, any divergence of ET partitioning is certainly an indicator that models may contain systematic errors in their formulations.

The mechanisms that govern the individual ET components of transpiration, soil evaporation, and canopy interception operate on varying spatial scales from relatively small (i.e. stomata, single plants) to larger regional scales (i.e. climate system) (Good et al., 2017; Pieruschka et al., 2010; Wang and Dickinson, 2012; Wang et al., 2014). Field methods for measuring transpiration typically measure at the scale of an individual leaf or plant (Rana and Katerji, 2000; Schlesinger and Jasechko, 2014). Such field techniques include: sap-flow measurements, diurnal water table changes, water-balance approaches, and isotope based approaches (Gibson and Edwards, 2002; Lautz, 2008; McJannet et al., 2007; Nizinski et al., 2011). Measurements from such studies are extrapolated to larger spatial scales through assumptions about the variability of sap-flux densities (Dye et al., 1991; Fernández et al., 2006), changes in isotopic composition of water within the plant (Brunel et al., 1997), and general homogeneity of vegetation and stomatal response to environmental conditions. The spatial scale of these measurements remains a limitation for ET partitioning validation, as research into regional hydrologic and climatic processes often requires estimates of partitioned fluxes at much larger spatial scales.

Furthermore, field studies of ET partitioning often focus on a single component such as transpiration or interception, and rarely attempt to estimate all contributing ET components. Canopy interception, for instance, is a well-developed field of study (Carlyle-Moses and Gash, 2011; Crockford and Richardson, 2000; Levia and Frost, 2006; Muzylo et al., 2009), and is often estimated as the difference between rainfall above and below the canopy. However, few canopy interception studies attempt to quantify the role of interception as part of the ET flux. Similarly, transpiration studies are often focused on the physiologic processes of vegetation and disregard the role of transpiration in larger hydrologic and atmospheric cycles. Some field methods do not directly measure soil evaporation, and instead quantify it as the residual of ET and transpiration. Due to the fractured nature of the ET partitioning research, few field studies are available quantifying transpiration, soil evaporation, and interception simultaneously.

To address the uncertainty surrounding ET partitioning in remote sensing-based ET models, we evaluate three models and their partitioning strategies against a compilation of field studies. We hope to contextualize partitioning comparisons made by Miralles et al. (2016) using empirical field methods. While previous studies have attempted to compare specific model estimates of either canopy interception or transpiration against field data, few have jointly assessed errors in remote sensing-based estimates against transpiration, soil evaporation, and interception. In comparing model performance against compiled field estimates we hope to (1) reconcile the deviations between each model partition against a field standard, (2) determine if the modeled errors are consistent or vary across different land surface or climate conditions, (3) identify assumptions or parameters within the model that contribute to error, (4) and contextualize some of the partitioning comparisons made by Miralles et al. (2016).

2. Methodology

We compared ET components from three remote sensing-based models against a compilation of field estimates of soil evaporation, transpiration, and interception. We assessed the Priestley-Taylor Jet Propulsion Lab model (PT-JPL)(Fisher et al., 2008), the Penman-Monteith MODerate Resolution Imaging Spectroradiometer (PM-MODIS) (Mu et al., 2011), and the Global Land Evaporation Amsterdam Model (GLEAM) (Martens et al., 2017; Miralles et al., 2011, 2010) model. Each model is widely used to estimate ET and provide relatively comparable estimates of the total ET flux (Miralles et al., 2016). Global annual mean values of ET for each model have been estimated at 54.9, 72.9, and $72.5 \times 10^3\,\mathrm{km}^3$ for PM-MOD, GLEAM, and PT-JPL respectively (Miralles et al., 2016).

2.1. Evaporation models

Each model evaluated for this study adopts a similar structure to estimate total ET fluxes as well as the individual components of ET. The model structure may be categorized into three separate functions: (1) quantifying potential ET, (2) partitioning the potential ET into its given components to be aggregated as total ET, and (3) translating the potential ET into an actual ET based on the constraints of the component processes. Different models employ different strategies in accomplishing these basic functions but individual model parameters often fall into a single categorical function.

2.1.1. Priestley-Taylor Jet Propulsion Lab (PT-JPL)

The PT-JPL model utilizes the Priestley-Taylor equation (Priestley and Taylor, 1972) to estimate potential ET flux and is described in depth in Fisher et al. (2008). The model uses ecophysiological and atmospheric constraints to reduce the potential ET flux to an actual ET flux. The total ET is partitioned between soil evaporation, E_s [m/s], canopy transpiration , E_v [m/s], and canopy interception, E_i [m/s] as

$$E_s = (f_{wet} + f_{SM}(1-f_{wet}))\alpha\frac{\Delta}{\lambda_v\rho_w(\Delta+\gamma)}(R_{ns}-G) \tag{1a}$$

$$E_v = (1-f_{wet})f_g f_T f_M\alpha\frac{\Delta}{\lambda_v\rho_w(\Delta+\gamma)}R_{nc} \tag{1b}$$

$$E_i = f_{wet}\alpha\frac{\Delta}{\lambda_v\rho_w(\Delta+\gamma)}R_{nc} \tag{1c}$$

where a is the Priestley-Taylor coefficient (considered equal to 1.26), Δ is the slope of the vapor pressure curve [Pa/K], γ is the psychrometric constant [Pa/K], R_n is the net radiation [W/m^2], G is the energy flux into the ground [W/m^2], λ_v is the latent heat of vaporization[J/kg], f_{wet} is a relative surface wetness parameter (see below), f_{SM} is the soil moisture constraint, f_g is the green canopy fraction, f_T is the plant temperature constraint, and f_M is the plant moisture constraint.

PT-JPL effectively accomplishes its partitioning using a canopy extinction equation to estimate the radiation penetrating through the canopy. This canopy extinction equation utilizes the leaf area index (LAI) in conjunction with the Beer-Lambert law of light attenuation (Norman Ay et al., 1995) to partition net radiation between the canopy and soil. Canopy processes (interception and transpiration) are determined using the radiation intercepted according to the Beer-Lambert equation, and soil evaporation is determined using the residual radiation penetrating the canopy.

PT-JPL scales each ET component by various scalars (f parameters) between 0 and 1 to account for environmental constraints on potential evaporation such as water and heat stress. Transpiration is constrained using four vegetation-based physiological parameters. Temperature and plant moisture effects on transpiration are calculated by normalizing phenological parameters by the maximum observed value per pixel. A canopy greenness fraction further constrains the transpiration flux based on the ratio between the fraction of absorbed photosynthetically active radiation (*fAPAR*) and the fraction of intercepted photosynthetically active radiation (*fIPAR*). The fourth constraint on transpiration is the surface wetness based on atmospheric relative humidity (f_{wet}). Soil evaporation constraints are determined by the surface wetness parameter (f_{wet}) and the available soil moisture (f_{sm}), the latter estimated by both relative humidity and vapor pressure deficit. Interception is estimated using the same f_{wet} parameter.

2.1.2. Penman-Monteith MODerate Resolution Imaging Spectroradiometer (PM-MODIS)

The PM-MOD model uses a framework based on the Penman-Monteith equation and utilizes specific conductance terms representing the vapor movement from the land surface to the overlying atmosphere. The model is described in depth by Mu et al. (2011) and estimates the components as:

$$E_i = f_{wet} f_c \frac{\Delta(R_n - G) + \rho c_p {}^{VPD}/_{r_a^{wc}}}{\lambda_v \rho_w (\Delta + \gamma \frac{r_s^{wc}}{r_a^{wc}})} \tag{2a}$$

$$E_v = (1 - f_{wet}) f_c \frac{\Delta(R_n - G) + \rho c_p {}^{VPD}/_{r_a^t}}{\lambda_v \rho_w (\Delta + \gamma \frac{r_s^t}{r_a^t})} \tag{2b}$$

$$E_s = \left[f_{wet} + (1 - f_{wet}) h^{VPD/\beta} \right] \frac{(s \times A_{soil} + \rho C_p (1 - f_c) {}^{VPD}/_{r_{as}})}{\lambda_v \rho_w (s + \gamma \frac{r_{tot}}{r_{as}})} \tag{2c}$$

Interception, transpiration, and soil evaporation are separated using fractional cover, f_c, calculated using *fAPAR*. The partitioned fluxes are constrained based on relative humidity (h), the fraction of wet surface (f_{wet}), and look-up table values of vegetation-dependent aerodynamic and surface resistances (r_a, r_s).

2.1.3. Global Land Evaporation Amsterdam Model (GLEAM)

Similarly to PT-JPL, GLEAM relies on a Priestley-Taylor framework to calculate potential ET. GLEAM uses a separate algorithm to calculate interception (E_i) based on a Gash analytical model (Gash, 1979; Valente et al., 1997) driven by precipitation observations. E_i estimates have been previously validated against field data independently (Miralles et al., 2010). The GLEAM model computes interception only for the tall canopy fraction within each pixel (see below).

Then soil evaporation (E_s), tall canopy transpiration (E_{tc})and short canopy transpiration (E_{sc}) are calculated as

$$E_s = f_s S_s \alpha_s \frac{\Delta}{\lambda_v \rho_w (\Delta + \gamma)} (R_n^s - G_s) \tag{3a}$$

$$E_{sc} = f_{sc} S_{sc} \alpha_{sc} \frac{\Delta}{\lambda_v \rho_w (\Delta + \gamma)} (R_n^{sc} - G_{sc}) \tag{3b}$$

$$E_{tc} = f_{tc} S_{tc} \alpha_{tc} \frac{\Delta}{\lambda_v \rho_w (\Delta + \gamma)} (R_n^{tc} - G_{tc}) - \beta E_i. \tag{3c}$$

The transpiration (E_v) is then calculated as the sum of E_{sc} and E_{tc}. In Eqs. (3a)–(3c), the partitioning of the evaporative flux into different components is based on the fractional vegetation cover (f). The fractional cover utilized is the MODIS Continuous Vegetation Fields product, MOD44B, which describes each pixel as a combination of bare soil, tall canopy, and short canopy vegetation (i.e. "s", "c", and "sc", respectively). The model uses vegetation-dependent parameterizations of G as well as different values of a for each vegetation cover type. Characteristic albedo ratios per vegetation cover type come from look up tables and determine how R_n is distributed per cover fraction.

GLEAM model constrains the Priestley and Taylor potential evaporation estimates based on an evaporative stress factor. This stress factors, S, is parameterized separately for the bare soil, tall canopy, and short vegetation components based on soil moisture and vegetation phenology for the vegetated fractions (see Ss, Stc and Ssc in Eqs. (3a)–(3c), respectively). The soil moisture is estimated based on a multilayer soil module driven by precipitation observations, and further optimized using a data assimilation system that incorporates observations of surface soil moisture (Martens et al., 2017, 2016). The transpiration stress associated with phenological changes is based on microwave vegetation optical depth, a proxy for vegetation water content (Miralles et al., 2011).

2.2. Field validation data

Field studies measuring the separate components of ET (i.e. soil evaporation, transpiration, and interception) are scarce. We utilized a set of studies previously consolidated by Schlesinger and Jasechko (2014) as well as additional studies containing annual values for transpiration and total ET. We then calculated soil evaporation as the residual of transpiration and total ET, assuming negligible interception. We compared the residual field estimate against modeled soil evaporation and the modeled residual (ET-T) and found that this assumption did not significantly influence the aggregate results of the study. These studies span several decades and use a variety of measurement techniques, primarily sap-flow measurements, isotope-based measurements, or meteorological models scaled using eddy-covariance and water balance models. Other studies have scaled measurements using biophysical models or through a water balance method to obtain canopy level values of transpiration and ET. Each field method suffers from their own set of assumption and is associated with some measurement error. Field study site locations are displayed in Fig. 1 and listed in Table 1. Despite the range of spatial support and uncertainty related to each technique in the dataset, we believe that, in the aggregate, the field estimates offer a good means to evaluate the performance of the model estimates.

Some field studies within the dataset span only the growing season of a given year and may overestimate the ratio of transpiration to ET on an annual scale. Other studies span several years and report a single annual estimate for transpiration and ET fluxes. Field estimates are reported as annual values and are compared against the modeled annual means. Instances existed where separate field studies reported values for the same pixel, in which case the field estimates were averaged.

The field studies described above largely ignore evaporation of rainfall intercepted by the canopy. To validate the interception components of the models we used the dataset previously used in the validation of the GLEAM interception loss estimates (Miralles et al., 2010). This dataset includes studies estimating the interception of forested canopies and excludes field sites in grasslands or shrublands where herbaceous interception may occur. The field dataset describes the interception at a given site as a mean annual depth per area of canopy. In order to estimate the interception in a given pixel, we scaled each field value using the fraction of forested land cover described by the MCD12C1 land cover fraction product [dataset] (NASA LP DAAC, Friedl and Sulla-Menashe, 2015). This does not account for the interception by herbaceous vegetation in non-forested areas, even though the rates of interception by short vegetation are expected to be comparatively much lower due to differences in aerodynamic conductance (David et al., 2005).

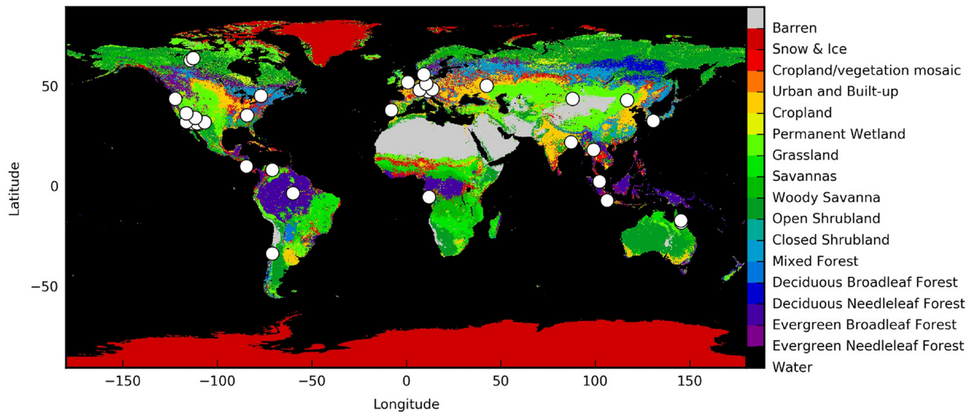

Fig. 1. Map of field study locations (white circles) and associated IGBP land cover types. Land cover is derived from the MODIS-based MCD12Q1 product.

2.3. Model forcing data

For those input variables that are common to all three models, we used the WAter Cycle Observation Multi-mission Strategy - ET forcing database (WACMOS-ET, http://wacmoset.estellus.eu/), which includes remote sensing derived surface meteorology and radiation fluxes (Michel et al., 2016; Miralles et al., 2016). In addition to the parameters already included in the WACMOS-ET forcing dataset, the PM-MOD model requires LAI, IGBP land cover, and *fAPAR* as inputs while the PT-JPL model requires NDVI. The original WACMOS-ET dataset contains LAI and *fAPAR* derived from the Joint Research Centre two-stream inversion package, but the values are not consistent with the MODIS derived LAI and *fAPAR* that both PM-MOD and PT-JPL require. We used MODIS vegetation products [dataset] (NASA LP DAAC, Didan, 2015) to supplement the WACMOS-ET data to force the PT-JPL and PM-MOD.

The input datasets vary in spatial and temporal resolution, but are re-sampled to a common 0.25° latitude × 0.25° longitude grid, and a 3-hourly temporal scale for PT-JPL and PM-MOD models, and a daily temporal scale for GLEAM. GLEAM no longer provides sub-daily estimates of ET, but PT-JPL requires maximum daily temperature and minimum daily humidity and is thus executed using the original 3-hourly forcing. In addition to the time variant fields, both GLEAM and PM-MOD require static fields. PM-MOD requires IGBP land cover values while GLEAM requires soil parameters derived from IGBP-DIS (Global Soil Data Task, 2014), and the MOD44B global vegetation continuous fields product.

3. Results & analysis

We compared the modeled estimates for each ET component against the field study estimates at each location. Table 2 lists the r^2 correlation coefficient, the standard error, the percent mean bias deviation (% MBD), and the percent root mean squared deviation (% RMSD) across different models. Fig. 2 shows linear regressions of the modeled estimates against the field estimates for each model and individual ET component.

Total ET results are comparable between models and show similar agreement with previous validations of total ET (Miralles et al., 2016). The modeled estimates generally overestimate the field estimates for small ET fluxes, and underestimate the field estimates at high values. Both PM-MOD and GLEAM show a tendency to underestimate the total flux, exhibiting a percent mean bias deviation (%MBD) of −21.6% and −20.9% respectively. PT-JPL ET estimates shows a %MBD of just −2.3%. The standard error exhibited by each model is very similar as are the overall trends. Comparatively, the modeled partitions show large discrepancies among themselves and agiant field data.

GLEAM offers the best results for estimating the transpiration flux, showing the lowest %RMSD, %MBD, and highest r^2 value. PT-JPL shows similar results to GLEAM for most statistics, except a lower correlation. The %MBD for the PM-MOD transpiration flux is −66.0%, which is substantially larger as compared to PT-JPL and GLEAM, where values of −10.7% and −5.4% are obtained respectively. The PT-JPL transpiration correlation (r^2 = 0.33) is much lower than previous validations of the transpiration component by Fisher et al. (2008) using sap flow estimates at three flux tower sites of alpine and sub-alpine climates. Compared to these three flux tower sites, our partitioning data spans a greater range of climate at a coarser temporal resolution. Recall that the slight underestimation of PT-JPL and GLEAM transpiration could be the result of certain field measurements reflecting only the growing season for a given year, rather than model deficiencies.

Both GLEAM (r^2 = 0.82) and PM-MOD (r^2 = 0.85) offer high correlations with field interception estimates. However, GLEAM shows lower RMSD (62.1%) and MBD (25.3%) as compared to PM-MOD (181.0% RMSD, 149.9% MBD). PT-JPL estimates of canopy interception compare poorly based on all statistical measures, resulting in an r^2 correlation of only 0.39 and a RMSD of 157.4%. Overall, estimates of interception showed a large level of divergence with the field estimates for both PM-MOD and PT-JPL. Model estimates showed especially large errors where field estimates exhibited small fluxes or where the fraction of forest within the pixel was determined to be small. However, the small number of field interception studies (N = 13) makes it difficult to definitively assess the model performance.

While the PT-JPL model provided the highest r^2 value and lowest RMSD for soil evaporation (89.8%RMSD, r^2 = 0.25), the results are relatively poor compared to the transpiration estimates. Modeled estimates of soil evaporation were inaccurate across all models and displayed little agreement with the field estimates. GLEAM, while exhibiting a low standard error (0.05), consistently underestimated the flux of soil evaporation compared to the field results (−45.6%MBD), which is mostly responsible for the bias in total ET exhibited by GLEAM. Conversely, PT-JPL estimates showed little bias (11.0%MBD) and a relatively high standard error (0.17). PM-MOD performed poorly across all statistical measures, exhibiting a positive bias (49.4%MBD).

Grouping the results by land cover type, water availability, and observational method allows us to identify how model performance changes across these groups. Fig. 3 shows the relative error for each model estimate against field estimates categorized by land cover type. We consolidated IGBP land cover values into four new groupings: forests (IGBP #1-5), shrublands (IGBP #6-7), grasslands (IGBP #8-10), and cropland and urban (IGBP # 0, 11-16). An analysis of each IGBP classification individually was impractical given the small number of values in each land cover group.

GLEAM, when analyzed across land cover, generally shows more variance in shrublands and grasslands and comparatively little variance in forests. This is most evident in the GLEAM model estimates of soil

Table 1
List of field studies used to validate the remote sensing model partitions. Shown are the study location, date, duration, and biome type along with the precipitation, transpiration, and evapotranspiration measured by each study. The potential evapotranspiration (PET), T/ET ratio, and aridity index are also listed. For each study, soil evaporation was calculated as the residual between the total ET and transpiration estimate of each study.

Reference	Start Date	End Date	Duration [days]	Location	Lat.	Long.	Forest Type	Method	Precip. [mm/yr]	E_v [mm/yr]	ET [mm/yr]	PET [mm/yr]	T/ET	Aridity
Poole et al. (1981)	Annual Mean	–	–	Chile	−33.07	−71.00	Mediterranean Shrubland	Xylem pressure potential	590	206.5	531	1388	0.39	0.43
McJannet et al. (2007)	9/13/2003	6/30/2005	656	Queensland	−17.45	145.50	LMCF	Sapflow	2983	591	1445	1476	0.41	1.83
McJannet et al. (2007)	9/13/2003	6/30/2005	656	Queensland	−17.45	145.50	LMRF	Sapflow + other	2420	591	1087	1476	0.54	1.83
McJannet et al. (2007)	8/9/2002	1/23/2004	532	Queensland	−16.53	145.28	LMCF	Sapflow	3040	579	1459	1513	0.40	1.94
McJannet et al. (2007)	8/9/2002	1/23/2004	532	Queensland	−16.53	145.28	LMRF	Sapflow + other	2833	579	882	1513	0.66	1.94
Calder et al. (1986)	4/6/1985	4/26/1985	20	Indonesia	−6.58	106.28	Tropical Rainforest	Model (with met. data), Isotopes	2851	883.81	1482.52	1591	0.60	1.79
Nizinski et al. (2011)	–	–	–	D.R. Congo	−4.69	12.08	Tropical Rainforest	Radial flow meter	1019	825.39	947.67	1375	0.87	0.74
Nizinski et al. (2011)	–	–	–	D.R. Congo	−4.69	12.08	Tropical Grassland	Radial flow meter	1019	591.02	703.11	1375	0.84	0.74
Leopoldo et al. (1995)	1/1/1981	12/31/1983	1094	Amazon	−3.13	−60.03	Tropical Rainforest	Model(with met. Data) Water Balance	2209	1243.7	1495	1612	0.83	1.29
Leopoldo et al. (1995)	1/1/1981	12/31/1983	1094	Brazil	−3.13	−60.03	Tropical Rainforest	Model(with met. Data) Water Balance	2209	1237.04	1480.03	1612	0.84	1.29
Salati and Vose (1984)	–	–	–	Brazil	−2.95	−59.95	Tropical Rainforest	Model(with met. Data) Water Balance	2000	1240	1620	1612	0.77	1.29
Salati and Vose (1984)	–	–	–	Brazil	−2.95	−59.95	Tropical Rainforest	Model(with met. Data) Water Balance	2000	980	1500	1612	0.65	1.29
Shuttleworth (1988)	9/1/1983	9/1/1985	731	Brazil	−2.95	−59.95	Tropical Rainforest	Model(with met. Data) Water Balance	2232	892.8	1116	1612	0.80	1.29
Tani et al., 2003	1/1/1996	12/31/1999	1460	Malaysia	2.97	102.30	Tropical lowland forest	Model (with met. data) Water Baland	1571	1218	1548	1689	0.79	0.93
Ataroff and Rada (2000)	1/1/1996	12/31/1998	1095	Venezuela	8.63	−71.03	TMCF	Micromet	4450	484	674	1011	0.72	4.40
Aparecido et al. (2016)	1/1/2014	12/31/2014	364	Costa Rica	10.39	−84.63	TMRF	Sapflow + other	4200	540	1004	1543	0.54	2.72
Tanaka et al. (2011)	1/1/1999	11/4/2002	1403	Thailand	18.80	98.90	LMCF	Sapflow	1768	626	812	1743	0.77	1.01
Banerjee in Galloux et al. (1981)	–	–	–	India	22.50	87.30	Tropical Rainforest	–	1623	730.35	1639.23	1617	0.45	1.00
Scott et al. (2006)	10/1/2003	10/31/2007	1491	United States	31.70	−110.40	Desert	Sap Flow	322	119.14	202.86	1516	0.59	0.21
Cavanaugh et al. (2011)	1/1/2008	12/31/2008	365	United States	31.74	−110.05	Desert	Model (with met. data), Sap flow	260	54.6	148.2	1567	0.42	0.17
Cavanaugh et al. (2011)	1/1/2008	12/31/2008	365	United States	31.91	−110.84	Desert	Model (with met. data), Sap flow	212	44.52	101.76	1460	0.47	0.15
Liu et al. (1995)	1/1/1992	12/31/1993	730	United States	31.95	−112.94	Desert	Model(with met. Data), Isotopes	200	160	200	1758	0.80	0.11
Schlesinger et al. (1987)	8/27/1983	7/17/1984	325	United States	32.52	−106.80	Desert	Water-balance; control and bare plots	210	151.2	210	1519	0.72	0.14
Poole et al. (1981)	9/1/1976	7/31/1977	333	United States	32.83	−116.43	Mediterranean Shrubland	Xylem pressure potential	475	152	394.25	1441	0.39	0.33
Kumagai et al. (2005)	4/1/2007	6/30/2008	456	Japan	33.13	130.72	Temperate Forest	Model (with met. data), sap flow	2128	486.2	911.4	949	0.53	2.24
McNulty et al. (1996)	Annual Mean	–	–	United States	34.00	−85.80	Temperate Forest	Xylem pressure potential	1225	600.25	784	1334	0.77	0.92
Waring et al. (1981)	–	–	–	United States	34.64	−111.78	Temperate Forest	Xylem pressure potential	1085	531.65	694.4	1349	0.76	0.80
Floret et al. (1982)	–	–	–	Tunisia	35.80	9.20	Steppe	Model (with met. data)	144	64.8	144	1533	0.45	0.11

(continued on next page)

Table 1 (*continued*)

Reference	Start Date	End Date	Duration [days]	Location	Lat.	Long.	Forest Type	Method	Precip. [mm/yr]	E_v [mm/yr]	ET [mm/yr]	PET [mm/yr]	T/ET	Aridity
Wilson et al. (2001)	1/1/1998	12/31/1998	364	United States	35.96	−84.29	Temperate Deciduous Forests	Model (with met. data), sap flow	1333	253.27	439.89	1242	0.58	1.07
Smith et al. (1995)	1/1/1988	12/31/1988	365	United States	36.93	−116.56	Desert	Xylem pressure potential	150	52.5	150	1431	0.35	0.10
Paço et al. (2009)	1/1/2005	12/31/2005	364	Portugal	38.50	−8.00	Temperate Deciduous Forests	Sap flow	669	488.37	669	1165	0.73	0.57
Huang et al. (2010)	1/1/2003	12/31/2006	1460	China	43.53	116.67	Steppe	Model (with met. data)	275	151.25	244.75	814	0.62	0.53
Hu et al. (2009)	1/1/2003	12/31/2005	1095	China	43.55	116.67	Temperate Grassland	Model (with met. data)	580	226.2	510.4	814	0.44	0.53
Waring et al. (1981)	10/1/1973	9/30/1974	364	United States	44.20	−122.30	Temperate Forest	Xylem pressure potential	2355	376.8	635.85	855	0.59	2.75
Liu et al. (2012)	1/1/2009	12/31/2009	364	China	44.28	87.93	Desert	Energy balance model	150	57	150	996	0.38	0.15
Telmer and Veizer (2000)	9/1/1991	9/30/1992	395	Canada	45.70	−76.90	Boreal Forest	Isotope-based (catchment)	872	392.4	462.16	842	0.85	1.04
Tajchman (1972)	1/1/1965	12/31/1965	364	Germany	48.04	11.56	Temperate Forest	Energy balance model	725	268.25	427.75	757	0.63	0.96
Granier et al. (2000)	1/1/1995	12/31/1995	364	France	48.67	7.08	Temperate Deciduous Forests	Sap flow	763	251.79	366.24	774	0.69	0.99
Pražák et al. (1994)	1/1/1985	12/31/1989	1825	Czech Republic	49.06	13.66	Temperate Forest	Model (with met. data)	366	190.32	384.3	739	0.52	0.50
Molchanov cited in Galloux et al. (1981)	–	–	–	Russia	50.75	42.50	Temperate Deciduous Forests	–	513	251.37	436.05	800	0.58	0.64
Two studies by Delfs (1967), cited by Choudhury and DiGirolamo (1998)	–	–	–	Germany	51.76	10.51	Boreal Forest	–	1237	235.03	556.65	675	0.42	1.83
Hudson (1988)	Annual Mean	–	–	United Kingdom	52.00	−3.50	Temperate Forest	Model (with met. data)	2620	183.4	786	566	0.23	4.63
Gash and Stewart (1977)	1/1/1975	12/31/1975	364	United Kingdom	52.42	0.67	Temperate Forest	Model (with met. data)	595	351.05	565.25	655	0.55	0.91
Ladekarl (1998)	7/1/1992	12/31/1994	913	Denmark	56.41	9.35	Temperate Deciduous Forests	Model (with met. data)	549	296.46	345.87	560	0.86	0.98
Gibson and Edwards (2002)	1/1/1993	12/31/1994	729	Canada	63.41	−114.26	Boreal Forest	Isotope-based (catchment)	340	241.4	302.6	423	0.81	0.80
Gibson and Edwards (2002)	1/1/1993	12/31/1994	729	Canada	64.50	−112.70	Tundra	Isotope-based (catchment)	310	105.4	130.2	354	0.81	0.88

Table 2
Validation statistics for different satellite-based ET datasets. The r^2 correlation coefficient describes the percent variability of the field data that the models were able to capture. The standard error describes the spread or standard deviation of the data. The mean bias error (MBD) describes the bias of the modeled estimate to either over- or under-estimate the field data. The root mean square deviation (RMSD) describes the accuracy of the model representing both the size and variation of the gross error. MBD and RMSD are reported as a percentage of the average field estimate for each partition. Blue represents good performance, while orange represents poor performance (For interpretation of the references to color in this table legend, the reader is referred to the web version of this article).

		Wacmos-ET Models 0.25° 2005-2007		
		PM-MOD	PT-JPL	GLEAM
r^2	E_s	0.14	0.25	0.14
	E_v	0.45	0.33	0.55
	E_i	0.85	0.39	0.82
	ET	0.64	0.75	0.61
Standard Error	E_s	0.19	0.17	0.05
	E_v	0.08	0.09	0.12
	E_i	0.19	0.34	0.09
	ET	0.09	0.07	0.08
% MBD	E_s	49.4	11.0	-45.6
	E_v	-66.0	-10.7	-5.4
	E_i	149.9	65.1	25.3
	ET	-21.6	-2.3	-20.9
% RMSD	E_s	114.2	89.8	90.6
	E_v	86.1	61.6	54.0
	E_i	181.0	157.4	62.1
	ET	45.1	35.1	48.5

evaporation, where the modeled estimates are extremely consistent in forests, less so in grasslands and croplands, and least in shrublands. As the GLEAM soil evaporation estimates become less consistent across these land cover types, the bias of these estimates shifts positively. A strong negative bias is evident in forests, and a positive one develops in shrublands. Similarly, the GLEAM model shows higher variance in its estimate errors of transpiration in shurblands and grasslands, and smaller variance in forests.

The differences between land cover types when considering interception become difficult to interpret because of the small amount of data in non-forested areas. The field interception dataset reports values exclusively from forests, so a non-forested land cover type for that location may suggest that the study site is not representative of the larger pixel. Apart from interception, PT-JPL and PM-MOD show little change in the bias of their estimates depending on land cover. Generally, all three models show a wider variation in estimate error in shrublands and grasslands than in forests.

Fig. 4 shows the relative estimate error of each model across different precipitation regimes. Each model shows large errors in interception at low precipitation, with PM-MOD exhibiting large sensitivity to annual precipitation. The relative error of the GLEAM soil evaporation trends negatively with increasing precipitation as does the PT-JPL estimate of total ET.

Fig. 5 shows the relative error of each model plotted by the field method used to partition ET. Estimates in soil evaporation are constant across field method, as are estimates in total ET to a lesser extent. Recall that soil evaporation is calculated as the residual of ET and transpiration, so that error in the observational method will be reflected in both transpiration and soil evaporation components. The PM-MOD transpiration estimates are also consistent, showing a clear negative bias regardless of field method. However, GLEAM and PT-JPL estimates vary slightly, while showing consistent estimates to one another.

4. Discussion

One of the inherent limitations in remote sensing-based evaluation studies is the challenge of acquiring independent observations that are representative of the scale of measurement. As such, we acknowledge that the spatial and temporal scale of the field-based estimates used in this study are not the ideal dataset for assessing the performance of these models, but few alternatives exists to estimate the individual components of ET. While eddy covariance observations are much better equipped for comparison with larger spatial fluxes and the finer temporal resolution of remote sensing-based ET products, they do not offer information regarding the individual components of ET. The field studies used in our analysis use a wide range of scaling techniques to acquire a canopy level ET measurement, and include eddy flux towers. Inevitably, some approaches are likely to be smaller in spatial scale than the satellite estimates, but, in the aggregate, still offer insight into how ET should be partitioned.

Our results show a moderate variation in total ET between each of the models, in agreement with previous studies (Michel et al., 2016; Miralles et al., 2016). However, the objective of this study is primarily the evaluation of the evaporation partitioning in these models. As large discrepancies exist between the separate fluxes estimated by different models, they are likely to overshadow the measurement error between field methods.

Clear patterns between modeled estimates are evident in the soil evaporation components of each model as well as the PM-MOD component of transpiration. This is illustrated in Fig. 5, where differences in modeled estimates are consistent regardless of the field method employed. PT-JPL and GLEAM estimates of transpiration show similar results, while varying slightly across different field methods. This highlights the difficulties in disentangling the results of PT-JPL and GLEAM transpiration, given the errors that may exist in the field data. As such, we will only discuss where clear differences between models exist or where the models show large biases with respect to the field data.

Through rooting uptake, plants are able to utilize water for transpiration held in the soil long after rain events. Soil evaporation and interception are much more dependent on transient rain events, which increase water storage in the canopy or upper layer of soil that becomes available for fast evaporation (Williams et al., 2004; Yepez et al., 2005). The available water source for either flux also depends on the connectivity of that water to surface water or deeper soil stores (Good et al., 2015). The differences in water sources for separate evaporation components changes the fundamental nature of those processes and the modeling techniques and data required to capture these physical processes. While fine temporal sampling may be required to capture rain events contributing to soil evaporation and interception, it may not be required to capture transpiration rates.

The modeled soil evaporation shows little correlation with field estimates across all models. In addition, both PT-JPL and PM-MOD show large standard error in their estimates of soil evaporation. While the inability of model routines to fully capture the physical process of soil evaporation might be responsible for part of the total error, differences in the spatial and temporal scales of soil evaporation as compared to transpiration may contribute to larger standard error in the results of soil evaporation. Soil moisture dynamics have shown to vary significantly in time and space depending on the antecedent conditions (Grayson et al., 1997). Moreover, changes in the lateral or vertical movement of water in soil associated with these changes could affect the connectivity to surface water flows and the availability of water for soil evaporation. Soil evaporation, being highly dependent on spatially variable soil moisture, could thus be disproportionately influenced by the differences in spatial scale between the field and modeled estimates. Additionally, different model representations of ground heat flux directly contribute to uncertainties in soil evaporation (Purdy et al., 2016).

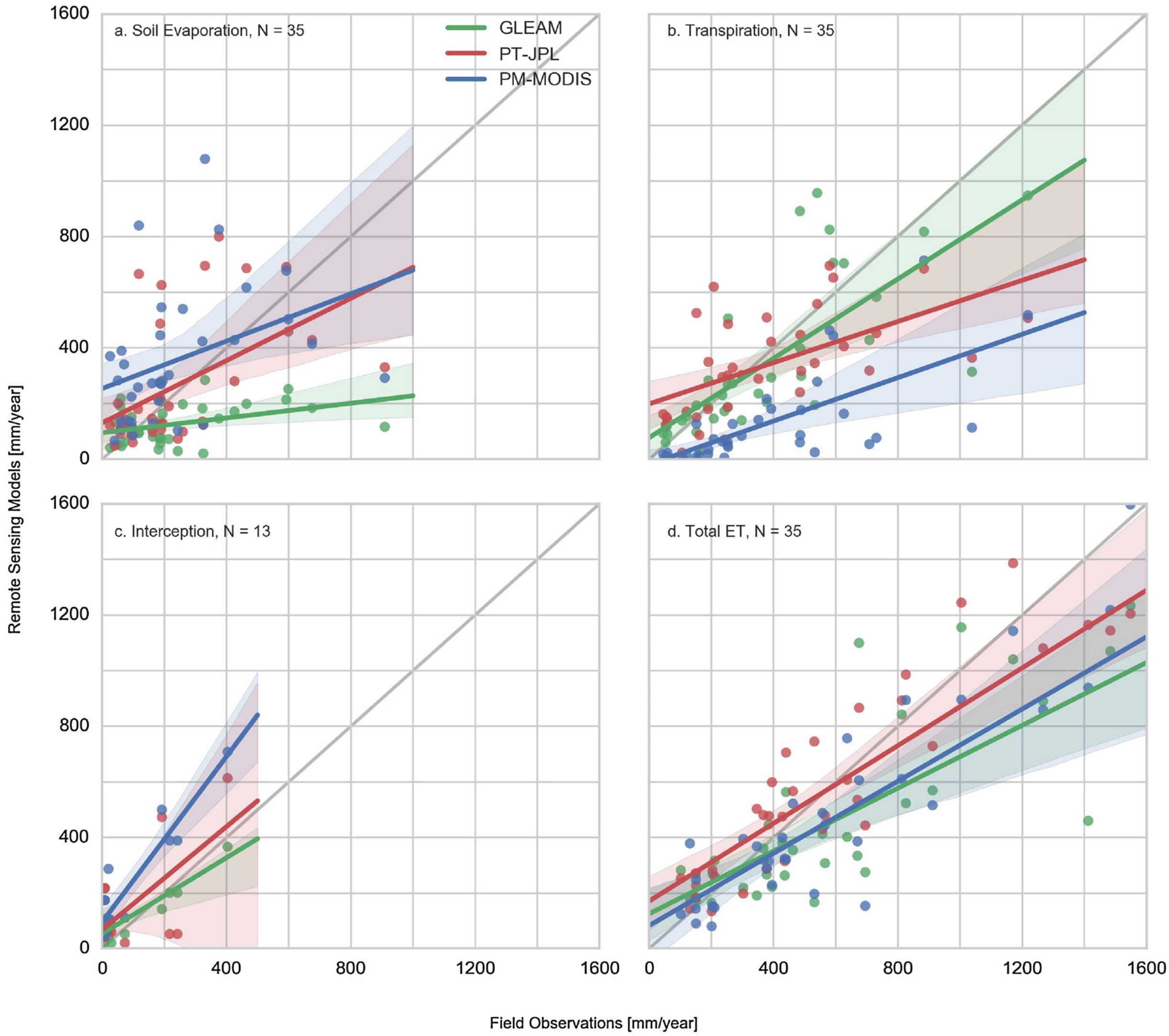

Fig. 2. Comparison between modeled ET estimates and field observed estimates for (a) soil evaporation, (b) transpiration, (c) interception, and (d) total ET flux for each model. A regression is plotted with the 95% confidence interval for each model shaded. The grey line represents a perfect fit between field and modeled results.

Estimates of soil evaporation from GLEAM clearly underestimate the field measurements. The relative error in soil evaporation estimates is highly correlated with the MOD44B products, showing a tendency to underestimate field measurements corresponding with areas of higher fraction of vegetation and lower bare soil. This arises due to the fact that GLEAM only considers soil evaporation from bare soil and does not estimate the soil evaporation occurring under the canopy or under herbaceous vegetation. The higher correlation of the estimate error with herbaceous vegetation than tall canopy suggests that the underestimation of soil evaporation by GLEAM is more significant in areas of herbaceous vegetation. Figs. 3 and 4 further corroborate this results. The underestimation in soil evaporation is most apparent in forested land cover and shows a negative relationship with increasing rainfall. As shown in Fig. 2, this causes most of the underestimation in the GLEAM estimates of total ET.

PM-MOD and PT-JPL share their approach to scale the soil evaporation using observations of relative humidity and vapor pressure deficit. As a result, they largely show similar estimates of soil evaporation, and similar validation statistics. Therefore, different parameters must cause the divergences found in the soil evaporation products of PT-JPL and PM-MOD. Differences in the Penman-Monteith and Priestley-Taylor models often depend on the parametrization of α in the Priestley-Taylor equation and resistance factors in the Penman-Monteith equation. The largest deviations between Penman-Monteith and Priestley-Taylor ET estimation occur when aerodynamic resistances and net radiation are small and VPD is high (Komatsu, 2005). Given the similarities between the model routines and output, it seems that the poor performance of the soil evaporation component likely stems from their shared assumptions.

PT-JPL and PM-MOD, by excluding precipitation and using relative humidity as a metric of a system's overall moisture, may see significant errors when soil and air moisture are in a state of disequilibrium. VPD and RH are correlated with soil moisture over weekly to seasonal time scales, but become decoupled over shorter time periods (Novick et al., 2016). Soil evaporation, more so than transpiration, may occur over shorter time periods following precipitation events. The use of humidity-based functions to account for water availability could explain the large standard error of the PM-MOD and PT-JPL soil evaporation component. However, spatial differences in the field and remote sensing-based products could also be culpable for the error. Higher frequency observations of ET partitioning are needed to better understand short-term dynamic changes in partitioning and how to reflect these dynamics within models.

Furthermore, soil moisture has been found to have a non-linear relationship with soil evaporation that can be characterized in two stages. The first stage is characterized by capillary transport, which

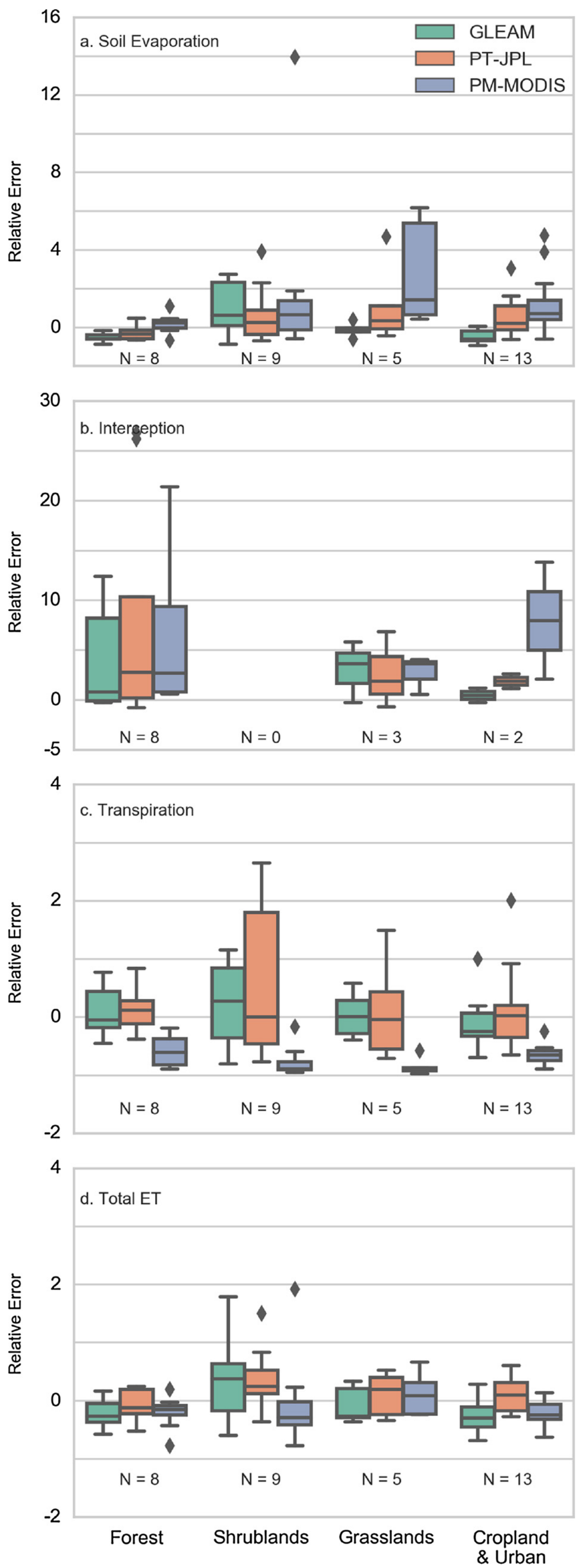

Fig. 3. Relative error between modeled and field estimates based on IGBP land cover type classification from MODIS using the WACMOS-ET dataset. The original IGBP land cover types were consolidated into four groups: Forests (IGBP 1–5), Shrublands (6–7), Grasslands (8–10), and Cropland and Urban (0, 10–16).

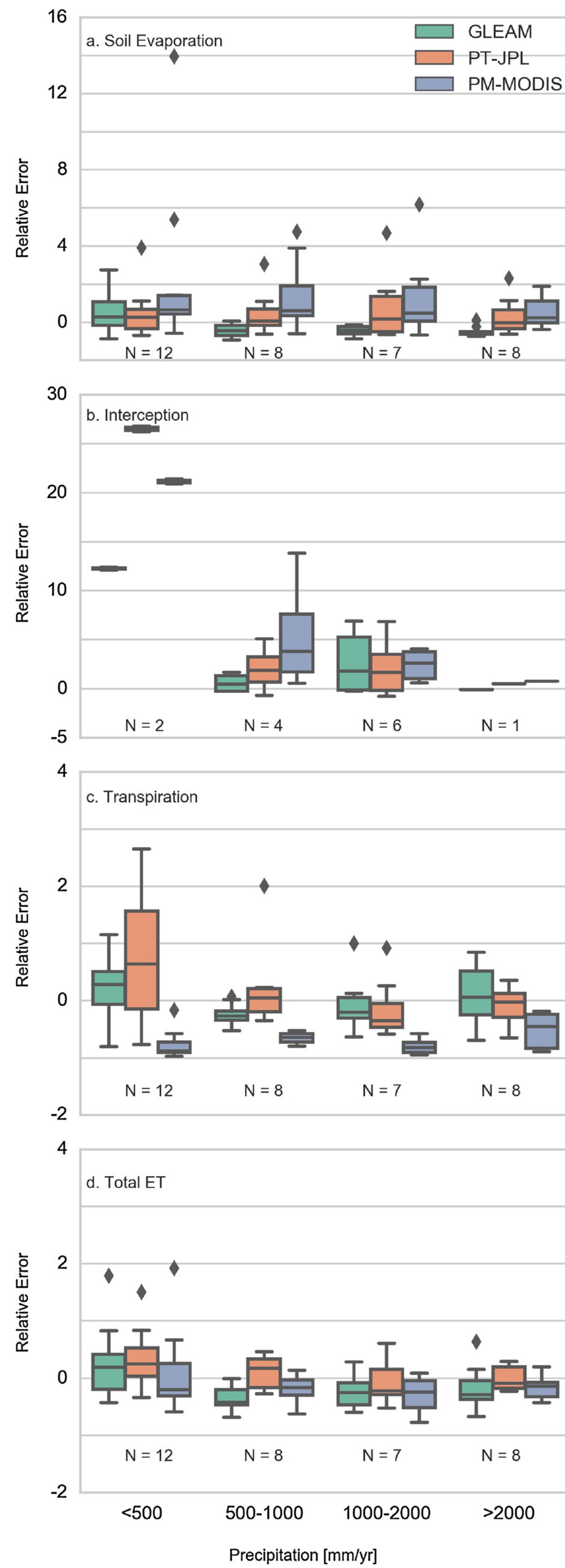

Fig. 4. Relative error between modeled and field estimates separated into different precipitation regimes using the WACMOS-ET dataset.

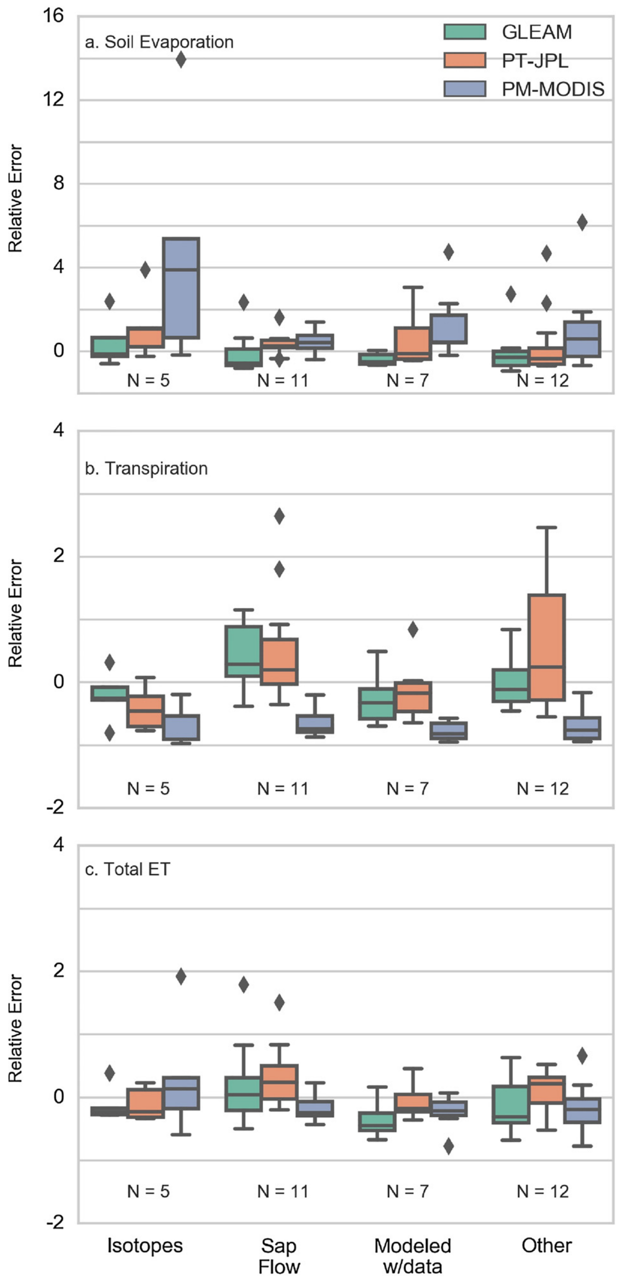

Fig. 5. Relative error between field and modeled estimates separated by field method type. The field methods are discretized into five groups: Isotopes, Sap Flow, Modeled using collected and meteorological data, modeled using no meteorological data, and a miscellaneous group.

sustains moisture at the soil surface. During the second stage, drying disrupts the hydraulic pathways within the soil and the vaporization plane moves below the soil surface, resulting in a significant reduction in soil evaporation (Haghighi and Or, 2013; Or et al., 2013). The point at which drying soils shift between stages of evaporation is largely dependent on physical soil characteristics and pore size and can cause dynamic shifts at hourly time scales in evaporation resistances (Aminzadeh and Or, 2017; Decker et al., 2017; Merlin et al., 2016). Neither PT-JPL nor PM-MOD consider soil properties in their estimate of soil evaporation, while GLEAM uses field capacity and wilting point to determine stress factors. The non-consideration of soil properties could be contributing to the large standard error in those soil evaporation estimates.

The transpiration estimates of both PT-JPL and GLEAM show better agreement with field estimates than their respective soil evaporation estimates. Partitioning research has shown transpiration to be the dominate flux of total ET (Jasechko et al., 2013). Therefore, the transpiration estimate of the model is critical in the models' ability to estimate total ET. Transpiration estimation and vegetation modeling represent research areas where remote sensing provides tremendous utility. The large degree of variability in plant species and size make ground measurements of canopy scale interaction difficult. The use of vegetation indices derived from remotely sensed products are much more advantageous for measuring heterogeneous vegetation and biophysical processes such as transpiration (Glenn et al., 2008).

PM-MOD strongly underestimates the transpiration flux estimated by field techniques. The only vegetation parameter used by PM-MOD is the fraction of absorbed photosynthetically active radiation, *fAPAR*, along with surface and aerodynamic resistances from the literature based on IGBP land cover type. These resistances can be very difficult to parameterize, and look-up table values do not reflect the temporal variability in these resistances. However, since the underestimation is consistent across all land cover types, it seems more likely that the use of *fAPAR* is driving the transpiration bias. Since PM-MOD uses *fAPAR* to partition radiation, the accuracy of the model may vary seasonally as phenology changes.

GLEAM performed very well at capturing the field interception estimates, as shown in previous studies (Miralles et al., 2010). Interception has been studied extensively, but little information exists on interception rates outside of densely forested ecosystems. While GLEAM models interception only for the tall canopy fraction of the pixel, the other models estimate interception outside of forests based on leaf area index and *fAPAR*. Interception losses outside of forests are likely small relative to total ET fluxes (David et al., 2005), but the value of including this interception remains unknown, given that few field measurements exist outside of forests.

Comparisons of interception estimates across Amazonia conducted by Miralles et al. (2016) found that PT-JPL and PM-MOD estimates (based on the WACMOS-ET vegetation properties as input) nearly doubled the interception rates of GLEAM and field-measured values found in the literature. Furthermore, interception has been shown to correlate strongly with both rainfall intensity and volume as they relate to canopy storage capacity (Pypker et al., 2005). PM-MOD and PT-JPL lack a canopy storage parameter, instead electing to use humidity as a proxy for surface wetness, and do not use precipitation as a forcing parameter. By not defining a storage capacity for the vegetation in PM-MOD and PT-JPL, the models could overestimate the flux for rain events exceeding the canopy storage. While PM-MOD and PT-JPL rely heavily on radiation as main driver of interception, field studies have shown that the flux of interception loss is partly decoupled from the available energy (Holwerda et al., 2011). In that sense, GLEAM likely provides better remote sensing-based estimates of interception, as it builds upon the knowledge gained in ground-based research on interception, which identifies vegetation characteristics and rainfall properties as the main determinants of the flux (Gash, 1979).

5. Conclusions

While this study attempted to validate the individual components of ET, little reliable data for these individual fluxes exists. Given the paucity of field datasets, it is difficult to draw definite conclusions on the sources of error within the modeled estimates of partitioned ET fluxes. While estimates diverge significantly between models, and modeled error is likely driving the bulk of the discrepancy with field partition estimates, the field methods themselves are also prone to errors. Furthermore, it is difficult to assess if the modeled estimates deviate due to the differences in model structure, or because of different forcing datasets and errors inherent in the forcing data. Given the multiple sources of potential error, it was challenging to determine to what magnitude we could attribute partitioning error to model methodology.

Remote sensing-based models will continue to play a dominant role in future ET research and its global implications (Fisher et al., 2017; Zhang et al., 2017). Improved spatial resolution and spectral availability of remote sensing products will undoubtedly provide a glut of modeled ET data for future researchers (Marshall et al., 2016; McCabe et al., 2017; Sun et al., 2017). However, the relative dearth of reliable field estimates for transpiration, soil evaporation, and interception inhibits quantifying the accuracy and applications of remote sensing-based ET estimates. Clearly, observations of the individual ET components are necessary to constrain ET models and improve ET accuracy for future research into climate and hydrologic dynamics. The consolidation of a global dataset of sap flux measurements (Poyatos et al., 2016) will undoubtedly present tremendous utility in validating remote sensing-based models and contribute to the advancement of ET science.

The results of this study present the first steps towards the validation of ET partitioning within remote sensing-based models. Our analysis shows that remote sensing-based ET models, despite showing similar and quite accurate total ET retrievals, produce estimates of individual components that deviate significantly from field measurements. Even for locations where the total ET is accurately modeled, the modeled components show significant deviations from observations. The uncertainty of the ET partitioning may cause model estimates to deteriorate when applied more broadly across space and time.

In particular, we find that:

- PM-MOD showed a strong negative bias in its transpiration estimate that caused a negative bias in the total ET estimate. The bias is likely related to the scaling parameters of the canopy, as PM-MOD relates the absorbed PAR linearly to the transpiration rate.
- Model estimates of soil evaporation showed little correlation with field estimates across all models. GLEAM exhibited a strong negative bias likely due to the non-consideration of below-canopy soil evaporation. Both PM-MOD and PT-JPL also exhibited large standard error in their estimates of soil evaporation.
- The quality of the interception estimates outside of forests was not assessed. GLEAM showed good agreement with the field data over forests, while PT-JPL and PM-MOD showed larger divergences. The non-consideration of rainfall and canopy storage capacity in PT-JPL and PM-MOD, and the direct dependency of interception loss on radiation, are the most likely causes for the disagreement with the field data.
- Finally, our results confirm that caution should be taken when applying any of these models in isolation, as long as the goal of the study relies heavily on the models partitioning of ET fluxes.

Data availability

The field observations and remote sensing datasets used in this study are all derived from previously published work.

The WACMOS-ET Reference Input Data Set was provided courtesy of the WACMOS-ET project and Estellus. http://wacmoset.estellus.eu/index.php?static9/data.

The MCD12C1 data product was retrieved from the online Data Pool, courtesy of the NASA Land Processes Distributed Active Archive Center (LP DAAC), USGS/Earth Resources Observation and Science (EROS) Center, Sioux Falls, South Dakota,

https://lpdaac.usgs.gov/data_access/data_pool.

The MOD15A2 data product was retrieved from the AppEEARS data page, courtesy of the NASA Earth Observing System Data and Information System(EOSDIS) and the Land Processing Distributed Active Archive Center (LP DAAC), USGS/Earth Resources Observation and Science (EROS) Center, Sioux Falls, South Dakota, https://lpdaacsvc.cr.usgs.gov/appeears.

Declarations of interest

None.

Acknowledgments

CT and SPG acknowledge the support of the Betty Minor scholarship. JBF contributed to this research from the Jet Propulsion Laboratory, California Institute of Technology, under a contract with the National Aeronautics and Space Administration. California Institute of Technology. Government sponsorship acknowledged. JBF was supported in part by NASA's SUSMAP, INCA, IDS, GRACE, and ECOSTRESS programs. MFM was supported by the King Abdullah University of Science and Technology. DGM acknowledges support from the European Research Council (ERC) under grant agreement n° 715254 (DRY–2–DRY). CJ acknowledges support from the EuropeanSpace Agency (ESA) under the project WACMOS-ET (Contract no. 4000106711/12/I-NB).

References

Aminzadeh, M., Or, D., 2017. Pore-scale study of thermal fields during evaporation from drying porous surfaces. Int. J. Heat Mass Transf. 104, 1189–1201. http://dx.doi.org/10.1016/J.IJHEATMASSTRANSFER.2016.09.039.

Anderson, M.C., Norman, J.M., Mecikalski, J.R., Otkin, J.A., Kustas, W.P., 2007. A climatological study of evapotranspiration and moisture stress across the continental United States based on thermal remote sensing: 1. Model formulation. J. Geophys. Res. 112, D10117. http://dx.doi.org/10.1029/2006JD007506.

Aparecido, L.M.T., Miller, G.R., Cahill, A.T., Moore, G.W., 2016. Comparison of tree transpiration under wet and dry canopy conditions in a Costa Rican premontane tropical forest. Hydrol. Process 30, 5000–5011. http://dx.doi.org/10.1002/hyp.10960.

Ataroff, M., Rada, F., 2000. Deforestation impact on water dynamics in a Venezuelan Andean cloud forest. AMBIO A J. Hum. Environ. 29, 440–444. http://dx.doi.org/10.1579/0044-7447-29.7.440.

Brunel, J.P., Walker, G.R., Dighton, J.C., Montenya, B., 1997. Use of stable isotopes of water to determine the origin of water used by the vegetation and to partition evapotranspiration. A case study from HAPEX-Sahel. J. Hydrol. 188–189, 466–481. http://dx.doi.org/10.1016/S0022-1694(96)03188-5.

Calder, I.R., Wright, I.R., Murdiyarso, D., 1986. A study of evaporation from tropical rain forest — West Java. J. Hydrol. 89, 13–31. http://dx.doi.org/10.1016/0022-1694(86)90139-3.

Carlyle-Moses, D.E., Gash, J.H.C., 2011. Rainfall Interception Loss by Forest Canopies. Springer, Dordrecht, pp. 407–423. http://dx.doi.org/10.1007/978-94-007-1363-5_20.

Cavanaugh, M.L., Kurc, S.A., Scott, R.L., 2011. Evapotranspiration partitioning in semiarid shrubland ecosystems: a two-site evaluation of soil moisture control on transpiration. Ecohydrology 4, 671–681. http://dx.doi.org/10.1002/eco.157.

Choudhury, B.J., DiGirolamo, N.E., 1998. A biophysical process-based estimate of global land surface evaporation using satellite and ancillary data I. Model description and comparison with observations. J. Hydrol. 205, 164–185. http://dx.doi.org/10.1016/S0022-1694(97)00147-9.

Crockford, R.H., Richardson, D.P., 2000. Partitioning of rainfall into throughfall, stemflow and interception: effect of forest type, ground cover and climate. Hydrol. Process. 14, 2903–2920. http://dx.doi.org/10.1002/1099-1085(200011/12)14:16/17<2903::AID-HYP126>3.0.CO;2-6.

David, J.S., Valente, F., Gash, J.H., 2005. Evaporation of intercepted rainfall. Encyclopedia of Hydrological Sciences. John Wiley & Sons, Ltd, Chichester, UK. http://dx.doi.org/10.1002/0470848944.hsa046.

Decker, M., Or, D., Pitman, A., Ukkola, A., 2017. New turbulent resistance parameterization for soil evaporation based on a pore-scale model: impact on surface fluxes in CABLE. J. Adv. Model. Earth Syst. 9, 220–238. http://dx.doi.org/10.1002/2016MS000832.

Delfs, J., 1967. Interception and stemflow in stands of Norway spruce and beech in West Germany. In: Sopper, W.E., Lull, H.W. (Eds.), Forest Hydrology. Pergamon Press, University Park Pennsylvania, pp. 179–185.

Didan, K., 2015. MOD13A2 MODIS/Terra Vegetation Indices 16-Day L3 Global 1km SIN Grid V006 [Data set]. NASA EOSDIS LP DAAC. http://dx.doi.org/10.5067/MODIS/MOD13A2.006.

Dye, P.J., Olbrich, B.W., Poulter, A.G., 1991. The influence of growth rings in Pinus patula on heat pulse velocity and sap flow measurement. J. Exp. Bot. 42, 867–870. http://dx.doi.org/10.1093/jxb/42.7.867.

Ek, M.B., Holtslag, A.A.M., 2004. Influence of soil moisture on boundary layer cloud development. J. Hydrometeorol. 5, 86–99. http://dx.doi.org/10.1175/1525-7541(2004)005<0086:IOSMOB>2.0.CO;2.

Ershadi, A., Mccabe, M.F., Evans, J.P., Wood, E.F., 2015. Impact of model structure and parameterization on Penman-Monteith type evaporation models. J. Hydrol. 525, 521–535. http://dx.doi.org/10.1016/j.jhydrol.2015.04.008.

Fernández, J.E., Durán, P.J., Palomo, M.J., Diaz-Espejo, A., Chamorro, V., Girón, I.F.,

2006. Calibration of sap flow estimated by the compensation heat pulse method in olive, plum and orange trees: relationships with xylem anatomy. Tree Physiol. 26, 719–728.

Fisher, J.B., Melton, F., Middleton, E., Hain, C., Anderson, M., Allen, R., McCabe, M.F., Hook, S., Baldocchi, D., Townsend, P.A., Kilic, A., Tu, K., Miralles, D.D., Perret, J., Lagouarde, J.-P., Waliser, D., Purdy, A.J., French, A., Schimel, D., Famiglietti, J.S., Stephens, G., Wood, E.F., 2017. The future of evapotranspiration: global requirements for ecosystem functioning, carbon and climate feedbacks, agricultural management, and water resources. Water Resour. Res. 53, 2618–2626. http://dx.doi.org/10.1002/2016WR020175.

Fisher, J.B., Tu, K.P., Baldocchi, D.D., 2008. Global estimates of the land–atmosphere water flux based on monthly AVHRR and ISLSCP-II data, validated at 16 FLUXNET sites. Remote Sens. Environ. 112, 901–919. http://dx.doi.org/10.1016/J.RSE.2007.06.025.

Floret, C., Pontanier, R., Rambal, S., 1982. Measurement and modelling of primary production and water use in a south tunisian steppe. J. Arid Environ. 77–90.

Friedl, M., Sulla-Menashe, D., 2015. MCD12C1 MODIS/Terra + Aqua Land Cover Type Yearly L3 Global 0.05Deg CMG V006 [Data set]. NASA EOSDIS Land Processes DAAC. http://dx.doi.org/10.5067/MODIS/MCD12C1.006.

Galloux, A., Benecke, P., Gietle, G., Hager, H., Kayser, C., Kiese, O., Knoerr, K.N., Murphy, C.E., Schnock, G., Sinclair, T.R., 1981. Radiation, heat, water and carbon dioxide balances. Dyn. Prop. For. Ecosyst. 87–204.

Gash, J.H.C., 1979. An analytical model of rainfall interception by forests. Q. J. R. Meteorol. Soc. 105, 43–55. http://dx.doi.org/10.1002/qj.49710544304.

Gash, J.H.C., Stewart, J.B., 1977. The evaporation from Thetford Forest during 1975. J. Hydrol . 35, 385–396. http://dx.doi.org/10.1016/0022-1694(77)90014-2.

Gibson, J.J., Edwards, T.W.D., 2002. Regional water balance trends and evaporation-transpiration partitioning from a stable isotope survey of lakes in northern Canada. Global Biogeochem. Cycles 16http://dx.doi.org/10.1029/2001GB001839. 10-1-10-14.

Glenn, E.P., Huete, A.R., Nagler, P.L., Nelson, S.G., 2008. Relationship between remotely-sensed vegetation indices, canopy attributes and plant physiological processes: what vegetation indices can and cannot tell us about the landscape. Sensors 8, 2136–2160. http://dx.doi.org/10.3390/s8042136.

Global Soil Data Task, 2014. Global Soil Data Products CD-ROM Contents (IGBP-DIS). Data Set. Available online [http://daac.ornl.gov] from Oak Ridge National Laboratory Distributed Active Archive Center, Oak Ridge, Tennessee, U.S.A. https://doi.org/10.3334/ORNLDAAC/565.

Good, S.P., Moore, G.W., Miralles, D.G., 2017. A mesic maximum in biological water use demarcates biome sensitivity to aridity shifts. Nat. Ecol. Evol. 1, 1883–1888. http://dx.doi.org/10.1038/s41559-017-0371-8.

Good, S.P., Noone, D., Bowen, G., 2015. Hydrologic connectivity constrains partitioning of global terrestrial water fluxes. Science 349, 175–177. http://dx.doi.org/10.1126/science.aaa5931.

Granier, A., Biron, P., Lemoine, D., 2000. Water balance, transpiration and canopy conductance in two beech stands. Agric. For. Meteorol. 100, 291–308. http://dx.doi.org/10.1016/S0168-1923(99)00151-3.

Grayson, R.B., Western, A.W., Chiew, F.H.S., Bloschl, G., 1997. Preferred states in spatial soil moisture patterns: local and nonlocal controls. Water Resour. Res. 33, 2897–2908.

Haghighi, E., Or, D., 2013. Evaporation from porous surfaces into turbulent airflows: coupling eddy characteristics with pore scale vapor diffusion. Water Resour. Res. 49, 8432–8442. http://dx.doi.org/10.1002/2012WR013324.

Hobbins, M.T., Ramírez, J.A., Brown, T.C., 2004. Trends in pan evaporation and actual evapotranspiration across the conterminous U.S.: paradoxical or complementary? Geophys. Res. Lett. http://dx.doi.org/10.1029/2004GL019846.

Holwerda, F., Bruijnzeel, L.A., Scatena, F.N., 2011. Comparison of passive fog gauges for determining fog duration and fog interception by a Puerto Rican elfin cloud forest. Hydrol. Process. 25, 367–373. http://dx.doi.org/10.1002/hyp.7641.

Hu, Z., Yu, G., Zhou, Y., Sun, X., Li, Y., Shi, P., Wang, Y., Song, X., Zheng, Z., Zhang, L., Li, S., 2009. Partitioning of evapotranspiration and its controls in four grassland ecosystems: Application of a two-source model. Agric. For. Meteorol. 149, 1410–1420. http://dx.doi.org/10.1016/J.AGRFORMET.2009.03.014.

Huang, X., Hao, Y., Wang, Y., Wang, Y., Cui, X., Mo, X., Zhou, X., 2010. Partitioning of evapotranspiration and its relation to carbon dioxide fluxes in Inner Mongolia steppe. J. Arid Environ 74, 1616–1623. http://dx.doi.org/10.1016/J.JARIDENV.2010.07.005.

Hudson, J.A., 1988. The contribution of soil moisture storage to the water balances of upland forested and grassland catchments. Hydrol. Sci. J 33, 289–309. http://dx.doi.org/10.1080/02626668809491249.

Huntington, T.G., 2006. Evidence for intensification of the global water cycle: review and synthesis. J. Hydrol. 319, 83–95. http://dx.doi.org/10.1016/J.JHYDROL.2005.07.003.

Jasechko, S., Sharp, Z.D., Gibson, J.J., Birks, S.J., Yi, Y., Fawcett, P.J., 2013. Terrestrial water fluxes dominated by transpiration. Nature 496, 347–350. http://dx.doi.org/10.1038/nature11983.

Komatsu, H., 2005. Forest categorization according to dry-canopy evaporation rates in the growing season: comparison of the Priestley-Taylor coefficient values from various observation sites. Hydrol. Process. 19, 3873–3896. http://dx.doi.org/10.1002/hyp.5987.

Kumagai, T., Saitoh, T.M., Sato, Y., Takahashi, H., Manfroi, O.J., Morooka, T., Kuraji, K., Suzuki, M., Yasunari, T., Komatsu, H., 2005. Annual water balance and seasonality of evapotranspiration in a Bornean tropical rainforest. Agric. For. Meteorol. 128, 81–92. http://dx.doi.org/10.1016/J.AGRFORMET.2004.08.006.

Ladekarl, U.L., 1998. Estimation of the components of soil water balance in a Danish oak stand from measurements of soil moisture using TDR. For. Ecol. Manage. 104, 227–238. http://dx.doi.org/10.1016/S0378-1127(97)00266-1.

Lautz, L.K., 2008. Estimating groundwater evapotranspiration rates using diurnal water-table fluctuations in a semi-arid riparian zone. Hydrogeol. J. 16, 483–497. http://dx.doi.org/10.1007/s10040-007-0239-0.

Lawrence, D.M., Thornton, P.E., Oleson, K.W., Bonan, G.B., Lawrence, D.M., Thornton, P.E., Oleson, K.W., Bonan, G.B., 2007. The partitioning of evapotranspiration into transpiration, soil evaporation, and canopy evaporation in a GCM: impacts on land–atmosphere interaction. J. Hydrometeorol. 8, 862–880. http://dx.doi.org/10.1175/JHM596.1.

Leopoldo, P.R., Franken, W.K., Villa Nova, N.A., 1995. Real evapotranspiration and transpiration through a tropical rain forest in central Amazonia as estimated by the water balance method. For. Ecol. Manage. 73, 185–195. http://dx.doi.org/10.1016/0378-1127(94)03487-H.

Levia, D.F., Frost, E.E., 2006. Variability of throughfall volume and solute inputs in wooded ecosystems. Prog. Phys. Geogr. 30, 605–632. http://dx.doi.org/10.1177/0309133306071145.

Littell, J.S., Peterson, D.L., Riley, K.L., Liu, Y., Luce, C.H., 2016. A review of the relationships between drought and forest fire in the United States. Global Change Biol. 22, 2353–2369. http://dx.doi.org/10.1111/gcb.13275.

Liu, B., Phillips, F., Hoines, S., Campbell, A.R., Sharma, P., 1995. Water movement in desert soil traced by hydrogen and oxygen isotopes, chloride, and chlorine-36, southern Arizona. J. Hydrol. 168, 91–110. http://dx.doi.org/10.1016/0022-1694(94)02646-S.

Liu, R., Li, Y., Wang, Q.-X., 2012. Variations in water and CO2 fluxes over a saline desert in western China. Hydrol. Process 26, 513–522. http://dx.doi.org/10.1002/hyp.8147.

Marshall, M., Thenkabail, P., Biggs, T., Post, K., 2016. Hyperspectral narrowband and multispectral broadband indices for remote sensing of crop evapotranspiration and its components (transpiration and soil evaporation). Agric. For. Meteorol. 218219, 122–134. http://dx.doi.org/10.1016/j.agrformet.2015.12.025.

Martens, B., Miralles, D., Lievens, H., Fernández-Prieto, D., Verhoest, N.E.C., 2016. Improving terrestrial evaporation estimates over continental Australia through assimilation of SMOS soil moisture. Int. J. Appl. Earth Obs. Geoinf. 48, 146–162. http://dx.doi.org/10.1016/J.JAG.2015.09.012.

Martens, B., Miralles, D.G., Lievens, H., van der Schalie, R., de Jeu, R.A.M., Fernández-Prieto, D., Beck, H.E., Dorigo, W.A., Verhoest, N.E.C., 2017. GLEAM v3: satellite-based land evaporation and root-zone soil moisture. Geosci. Model Dev. 10, 1903–1925. http://dx.doi.org/10.5194/gmd-10-1903-2017.

McCabe, M.F., Aragon, B., Houborg, R., Mascaro, J., 2017. CubeSats in hydrology: ultrahigh-resolution insights into vegetation dynamics and terrestrial evaporation. Water Resour. Res. 53, 10017–10024. http://dx.doi.org/10.1002/2017WR022240.

Mccabe, M.F., Ershadi, A., Jimenez, C., Miralles, D.G., Michel, D., Wood, E.F., 2016. The GEWEX LandFlux project: evaluation of model evaporation using tower-based and globally gridded forcing data. Geosci. Model Dev. 9, 283–305. http://dx.doi.org/10.5194/gmd-9-283-2016.

McJannet, D., Fitch, P., Disher, M., Wallace, J., 2007. Measurements of transpiration in four tropical rainforest types of north Queensland, Australia. Hydrol. Process. 21, 3549–3564. http://dx.doi.org/10.1002/hyp.6576.

McNulty, S.G., Vose, J.M., Swank, W.T., 1996. Loblolly pine hydrology and productivity across the southern United States. For. Ecol. Manage. 86, 241–251. http://dx.doi.org/10.1016/S0378-1127(96)03744-9.

Merlin, O., Stefan, V.G., Amazirh, A., Chanzy, A., Ceschia, E., Er-Raki, S., Gentine, P., Tallec, T., Ezzahar, J., Bircher, S., Beringer, J., Khabba, S., 2016. Modeling soil evaporation efficiency in a range of soil and atmospheric conditions using a meta-analysis approach. Water Resour. Res. http://dx.doi.org/10.1002/2015WR018233.

Michel, D., Jiménez, C., Miralles, D.G., Jung, M., Hirschi, M., Ershadi, A., Martens, B., Mccabe, M.F., Fisher, J.B., Mu, Q., Seneviratne, S.I., Wood, E.F., Fernández-Prieto, D., 2016. The WACMOS-ET project – part 1: tower-scale evaluation of four remote-sensing-based evapotranspiration algorithms. Hydrol. Earth Syst. Sci. 20, 803–822. http://dx.doi.org/10.5194/hess-20-803-2016.

Miralles, D.G., Gash, J.H., Holmes, T.R.H., De Jeu, R.A.M., Dolman, A.J., 2010. Global canopy interception from satellite observations. J. Geophys. Res. 115. http://dx.doi.org/10.1029/2009JD013530.

Miralles, D.G., Holmes, T.R.H., De Jeu, R.A.M., Gash, J.H., Meesters, A.G.C.A., Dolman, A.J., 2011. Global land-surface evaporation estimated from satellite-based observations. Hydrol. Earth Syst. Sci. 15, 453–469. http://dx.doi.org/10.5194/hess-15-453-2011.

Miralles, D.G., Jiménez, C., Jung, M., Michel, D., Ershadi, A., McCabe, M.F., Hirschi, M., Martens, B., Dolman, A.J., Fisher, J.B., Mu, Q., Seneviratne, S.I., Wood, E.F., Fernaìndez-Prieto, D., 2016. The WACMOS-ET project – part 2: evaluation of global terrestrial evaporation data sets. Hydrol. Earth Syst. Sci. Discuss. 12, 10651–10700. http://dx.doi.org/10.5194/hessd-12-10651-2015.

Molden, D., Oweis, T., Steduto, P., Bindraban, P., Hanjra, M.A., Kijne, J., 2010. Improving agricultural water productivity: between optimism and caution. Agric. Water Manag. 97, 528–535. http://dx.doi.org/10.1016/J.AGWAT.2009.03.023.

Mu, Q., Zhao, M., Running, S.W., 2011. Improvements to a MODIS global terrestrial evapotranspiration algorithm. Remote Sens. Environ. 115, 1781–1800. http://dx.doi.org/10.1016/j.rse.2011.02.019.

Muzylo, A., Llorens, P., Valente, F., Keizer, J.J., Domingo, F., Gash, J.H.C., 2009. A review of rainfall interception modelling. J. Hydrol. 370, 191–206. http://dx.doi.org/10.1016/J.JHYDROL.2009.02.058.

Nizinski, J.J., Galat, G., Galat-Luong, A., 2011. Water balance and sustainability of eucalyptus plantations in the Kouilou basin (Congo-Brazzaville). Russ. J. Ecol. 42, 305–314. http://dx.doi.org/10.1134/S1067413611040126.

Norman Ay, J.M., Kustas, W.P., Humes, K.S., 1995. Source approach for estimating soil and vegetation energy fluxes in observations of directional radiometric surface

temperature. Agric. For. Meteorol. 77, 263–293.
Novick, K.A., Ficklin, D.L., Stoy, P.C., Williams, C.A., Bohrer, G., Oishi, A.C., Papuga, S.A., Blanken, P.D., Noormets, A., Sulman, B.N., Scott, R.L., Wang, L., Phillips, R.P., 2016. The increasing importance of atmospheric demand for ecosystem water and carbon fluxes. Nat. Clim. Change 6, 1023–1027. http://dx.doi.org/10.1038/nclimate3114.
Oki, T., Kanae, S., 2006. Global hydrological cycles and world water resources. Science 313, 1068–1072. http://dx.doi.org/10.1126/science.1128845.
Or, D., Lehmann, P., Shahraeeni, E., Shokri, N., 2013. Advances in soil evaporation physics—a review. Vadose Zone J. 12, 0. http://dx.doi.org/10.2136/vzj2012.0163.
Paço, T.A., David, T.S., Henriques, M.O., Pereira, J.S., Valente, F., Banza, J., Pereira, F.L., Pinto, C., David, J.S., 2009. Evapotranspiration from a Mediterranean evergreen oak savannah: the role of trees and pasture. J. Hydrol. 369, 98–106. http://dx.doi.org/10.1016/J.JHYDROL.2009.02.011.
Pielke, R.A., Avissar, R., Raupach, M., Dolman, A.J., Zeng, X., Denning, A.S., 1998. Interactions between the atmosphere and terrestrial ecosystems: influence on weather and climate. Global Change Biol. 4, 461–475. http://dx.doi.org/10.1046/j.1365-2486.1998.t01-1-00176.x.
Pieruschka, R., Huber, G., Berry, J.A., 2010. Control of transpiration by radiation. Proc. Natl. Acad. Sci. U. S. A. 107, 13372–13377. http://dx.doi.org/10.1073/pnas.0913177107.
Poole, D.K., Roberts, S.W., Miller, P.C., 1981. Water utilization. In: Miller, P.C. (Ed.), Resources Use by Chaparral and Matorral. Springer-Verlag, New York, pp. 123–149.
Poyatos, R., Granda, V., Molowny-Horas, R., Mencuccini, M., Steppe, K., Martínez-Vilalta, J., 2016. SAPFLUXNET: towards a global database of sap flow measurements. Tree Physiol. 36, 1449–1455. http://dx.doi.org/10.1093/treephys/tpw110.
Pražák, J., Šír, M., Tesařr, M., 1994. Estimation of plant transpiration from meteorological data under conditions of sufficient soil moisture. J. Hydrol. 162, 409–427. http://dx.doi.org/10.1016/0022-1694(94)90239-9.
Priestley, C.H.B., Taylor, R.J., 1972. On the assessment of sruface heat flux and evaporation using large scale parameters. Mon. Weather Rev. 81–92.
Purdy, A.J., Fisher, J.B., Goulden, M.L., Famiglietti, J.S., 2016. Ground heat flux: an analytical review of 6 models evaluated at 88 sites and globally. J. Geophys. Res. Biogeosci. 121, 3045–3059. http://dx.doi.org/10.1002/2016JG003591.
Pypker, T.G., Bond, B.J., Link, T.E., Marks, D., Unsworth, M.H., 2005. The importance of canopy structure in controlling the interception loss of rainfall: examples from a young and an old-growth Douglas-fir forest. Agric. For. Meteorol. 130, 113–129. http://dx.doi.org/10.1016/J.AGRFORMET.2005.03.003.
Rana, G., Katerji, N., 2000. Measurement and estimation of actual evapotranspiration in the field under Mediterranean climate: a review. Eur. J. Agron. 13, 125–153. http://dx.doi.org/10.1016/S1161-0301(00)00070-8.
Salati, E., Vose, P.B., 1984. Amazon Basin: a system in equilibrium. Science 225, 129–138. http://dx.doi.org/10.1126/science.225.4658.129. (80-).
Schlesinger, W.H., Fonteyn, P.J., Marion, G.M., 1987. Soil moisture content and plant transpiration in the Chihuahuan Desert of New Mexico. J. Arid Environ. 12, 119–126.
Schlesinger, W.H., Jasechko, S., 2014. Transpiration in the global water cycle. Agric. For. Meteorol. 189–190, 115–117. http://dx.doi.org/10.1016/j.agrformet.2014.01.011.
Schmugge, T.J., Kustas, W.P., Ritchie, J.C., Jackson, T.J., Rango, A., 2002. Remote sensing in hydrology. Adv. Water Resour. 25, 1367–1385. http://dx.doi.org/10.1016/S0309-1708(02)00065-9.
Scott, R.L., Huxman, T.E., Cable, W.L., Emmerich, W.E., 2006. Partitioning of evapotranspiration and its relation to carbon dioxide exchange in a Chihuahuan Desert shrubland. Hydrol. Process 20, 3227–3243. http://dx.doi.org/10.1002/hyp.6329.
Seneviratne, S.I., Corti, T., Davin, E.L., Hirschi, M., Jaeger, E.B., Lehner, I., Orlowsky, B., Teuling, A.J., 2010. Investigating soil moisture–climate interactions in a changing climate: a review. Earth-Sci. Rev. 99, 125–161. http://dx.doi.org/10.1016/J.EARSCIREV.2010.02.004.
Shukla, J., Mintz, Y., 1982. Influence of land-surface evapotranspiration on the earth's climate. Science 215, 1498–1501. http://dx.doi.org/10.1126/science.215.4539.1498.
Shuttleworth, W.J., 1988. Evaporation from amazonian rainforest. Proc. R. Soc. B Biol. Sci. 233, 321–346. http://dx.doi.org/10.1098/rspb.1988.0024.
Smith, S.D., Herr, C.A., Learyt, K.L., Piorkowski, J.M., 1995. Soil-plant water relations in a Mojave Desert mixed shrub community: a comparison of three geomorphic surfaces. J. Arid Environ. 29, 339–351.
Sun, L., Anderson, M.C., Gao, F., Hain, C., Alfieri, J.G., Sharifi, A., McCarty, G.W., Yang, Y., Yang, Y., Kustas, W.P., McKee, L., 2017. Investigating water use over the Choptank River Watershed using a multisatellite data fusion approach. Water Resour. Res. 53, 5298–5319. http://dx.doi.org/10.1002/2017WR020700.
Tajchman, S.J., 1972. The radiation and energy balances of coniferous and deciduous forests. J. Appl. Ecol. 9, 359. http://dx.doi.org/10.2307/2402437.
Tanaka, N., Kuraji, K., Tantasirin, C., Takizawa, H., Tangtham, N., Suzuki, M., 2011. Relationships between rainfall, fog and throughfall at a hill evergreen forest site in northern Thailand. Hydrol. Process 25, 384–391. http://dx.doi.org/10.1002/hyp.7729.
Tani, M., Rah Nik, A.I., Yasuda, Y., Shamsuddin, S., Sahat, M., Takanashi, S., 2003. Long-term estimation of evapotranspiration from a tropical rain forest in Peninsular Malaysia. Water Resour. Syst. Availab. Glob Chang.
Telmer, K., Veizer, J., 2000. Isotopic constraints on the transpiration, evaporation, energy, and gross primary production Budgets of a large boreal watershed: ottawa river basin, Canada. Global Biogeochem. Cycles 14, 149–165. http://dx.doi.org/10.1029/1999GB900078.
Teuling, A.J., Hirschi, M., Ohmura, A., Wild, M., Reichstein, M., Ciais, P., Buchmann, N., Ammann, C., Montagnani, L., Richardson, A.D., Wohlfahrt, G., Seneviratne, S.I., 2009. A regional perspective on trends in continental evaporation. Geophys. Res. Lett. 36http://dx.doi.org/10.1029/2008GL036584. n/a-n/a.
Trenberth, K.E., 2011. Changes in precipitation with climate change. Clim. Res. http://dx.doi.org/10.2307/24872346.
Valente, F., David, J.S., Gash, J.H.C., 1997. Modelling interception loss for two sparse eucalypt and pine forests in central Portugal using reformulated Rutter and Gash analytical models. J. Hydrol. 190, 141–162. http://dx.doi.org/10.1016/S0022-1694(96)03066-1.
Wallace, J., 2000. Increasing agricultural water use efficiency to meet future food production. Agric. Ecosyst. Environ. 82, 105–119. http://dx.doi.org/10.1016/S0167-8809(00)00220-6.
Wang, K., Dickinson, R.E., 2012. A review of global terrestrial evapotranspiration: observation, modeling, climatology, and climatic variability. Rev. Geophys. 50. http://dx.doi.org/10.1029/2011RG000373.
Wang, L., Good, S.P., Caylor, K.K., 2014. Global synthesis of vegetation control on evapotranspiration partitioning. Geophys. Res. Lett. 41, 6753–6757. http://dx.doi.org/10.1002/2014GL061439.
Waring, R.H., Rogers, J.J., Swank, W.T., 1981. Water Relations and Hydrologic Cycles. Cambridge University Press, Cambridge.
Williams, D.G., Cable, W., Hultine, K., Hoedjes, J.C.B., Yepez, E.A., Simonneaux, V., Er-Raki, S., Boulet, G., de Bruin, H.A.R., Chehbouni, A., Hartogensis, O.K., Timouk, F., 2004. Evapotranspiration components determined by stable isotope, sap flow and eddy covariance techniques. Agric. For. Meteorol. 125, 241–258. http://dx.doi.org/10.1016/J.AGRFORMET.2004.04.008.
Wilson, K.B., Hanson, P.J., Mulholland, P.J., Baldocchi, D.D., Wullschleger, S.D., 2001. A comparison of methods for determining forest evapotranspiration and its components: sap-flow, soil water budget, eddy covariance and catchment water balance. Agric. For. Meteorol. 106, 153–168. http://dx.doi.org/10.1016/S0168-1923(00)00199-4.
Yepez, E.A., Huxman, T.E., Ignace, D.D., English, N.B., Weltzin, J.F., Castellanos, A.E., Williams, D.G., 2005. Dynamics of transpiration and evaporation following a moisture pulse in semiarid grassland: a chamber-based isotope method for partitioning flux components. Agric. For. Meteorol. 132, 359–376. http://dx.doi.org/10.1016/j.agrformet.2005.09.006.
Zhang, Y., Chiew, F.H.S., Peña-Arancibia, J., Sun, F., Li, H., Leuning, R., 2017. Global variation of transpiration and soil evaporation and the role of their major climate drivers. J. Geophys. Res. Atmos. 122, 6868–6881. http://dx.doi.org/10.1002/2017JD027025.
Zhang, Y., Peña-Arancibia, J.L., McVicar, T.R., Chiew, F.H.S., Vaze, J., Liu, C., Lu, X., Zheng, H., Wang, Y., Liu, Y.Y., Miralles, D.G., Pan, M., 2016. Multi-decadal trends in global terrestrial evapotranspiration and its components. Sci. Rep. 6, 19124. http://dx.doi.org/10.1038/srep19124.